

Luminescence chronology of reticulated laterites in the humid subtropical mountains of South China

Jianhui Jin¹, Junjie Qiu², Zhiyong Ling³, Junjie Wei², Xinxin Zuo², Zhizhong Li²,
Chenyang Hou², and Daiyu Xu²

¹FUJIAN NORMAL UNIVERSITY

²Fujian normal university

³Qinghai Institute of Salt lake, Chinese Academy Sciences

December 17, 2022

Abstract

Laterite is a red weathering crust developed with various rocks and Quaternary loose sediments as its parent material in the tropics and subtropics regions of the world, and it is also the most widely distributed Quaternary earthy accumulation in China. Since the 1930s, most researchers have believed that the fluvial reticulated laterite in southern China was influenced by the warm and humid climate of the Middle Pleistocene. In recent years, the remains of Paleolithic human activities are often found in the reticulated laterite of southern China. However, the study of laterite chronology is sporadic or there is no critical chronological analysis, which causes uncertainty in the identification and discussion of the ages of reticulated laterite and Paleolithic sites in South China. In this study, a paleolithic site found in fluvial reticulated laterite in South China was systematically tested by quartz optical luminescence dating and geomorphic process analysis. The results show that, (1) The T3 terrace, an archive of hominin activity in the study area, primarily formed between 56 and 11 ka. (2) Reticulated laterite cannot be used simply to determine the ages of the Paleolithic sites found in this stratum, and typical reticulated laterite cannot be used as a marker for climatic stratigraphy and chronostratigraphy. The fluvial reticulated laterite in the southern tropics, under suitable hydrothermal conditions, can form within tens of thousands of years or even within 10 ka. (3) Human activities can also lead to an inversion in the age of reticulated red soil.

Hosted file

952269_0_art_file_10541187_rmyp71.docx available at <https://authorea.com/users/567123/articles/613617-luminescence-chronology-of-reticulated-laterites-in-the-humid-subtropical-mountains-of-south-china>

1
2 **Luminescence chronology of reticulated laterites in the humid**
3 **subtropical mountains of South China**

4
5 Jin Jianhui^{1,2,3*}, Qiu Junjie¹, Ling Zhiyong³, Wei Junjie¹, Zuo Xinxin^{1,2}, Li Zhizhong¹,
6 Hou Chenyang¹, Xu Daiyu¹

7
8 1. Key Laboratory of Subtropical Resources and Environment of Fujian Province, Fujian Normal University,
9 Fuzhou, 350007, China

10 2. Centre for Southeast Environmental Archaeology of China, Fujian Normal University, Pingtan, 350400, China

11 3. Qinghai Institute of Salt Lake, Chinese Academy Sciences, Xi'ning, 810008, China

12 *
13 **Corresponding author: Jin Jianhui, E-mail: geojjh@fjnu.edu.cn**

14 **Abstract:** Laterite is a red weathering crust developed with various rocks and Quaternary loose
15 sediments as its parent material in the tropics and subtropics regions of the world, and it is also the
16 most widely distributed Quaternary earthy accumulation in China. Since the 1930s, most
17 researchers have believed that the fluvial reticulated laterite in southern China was influenced by
18 the warm and humid climate of the Middle Pleistocene. In recent years, the remains of Paleolithic
19 human activities are often found in the reticulated laterite of southern China. However, the study
20 of laterite chronology is sporadic or there is no critical chronological analysis, which causes
21 uncertainty in the identification and discussion of the ages of reticulated laterite and Paleolithic
22 sites in South China. In this study, a paleolithic site found in fluvial reticulated laterite in South
23 China was systematically tested by quartz optical luminescence dating and geomorphic process
24 analysis. The results show that, (1) The T₃ terrace, an archive of hominin activity in the study area,
25 primarily formed between 56 and 11 ka. (2) Reticulated laterite cannot be used simply to
26 determine the ages of the Paleolithic sites found in this stratum, and typical reticulated laterite
27 cannot be used as a marker for climatic stratigraphy and chronostratigraphy. The formation time of
28 the reticulated laterite varied significantly between different sedimentary facies. The fluvial
29 reticulated laterite in the southern tropics, under suitable hydrothermal conditions, can form within
30 tens of thousands of years or even within 10 ka. (3) Human activities can affect the burial age of
31 reticulated red soil, and the temporal nature of riverine terraces can also lead to an inversion in the
32 age of reticulated red soil.

33 **Keywords:** Laterite; Luminescence dating; Paleolithic site; Humid subtropics; South China;

34 **1. Introduction**

35 Laterite in southern China is distributed from the north to the south of the Qinling Mountain–
36 Huaihe River line and from the west to the east of Tibet (Yuan et al., 2008). Information on the
37 geology, environment, climate, and Paleolithic culture of the area is abundantly available. Since
38 the Quaternary, the area south of the Qinling Mountain–Huaihe River line has experienced a long
39 period of tropical and subtropical climates. Red weathering crusts of different thicknesses have
40 been developed and preserved on the upper parts of various rocks and loose sediments, covering
41 an area of more than $200 \times 10^4 \text{ km}^2$ (Fig. 1).

42 The development of weathering crusts is controlled by parent material, climate, topography,
43 hydrology, and time. The lithologic characteristics of weathering crusts vary significantly under
44 the combination and control of different factors. However, their natural disadvantage is the lack of
45 paleontological fossils, which makes it difficult to study the stratigraphy, environment, and
46 paleohuman evolution. Since the 1970s, researchers have applied newly developed dating
47 techniques to study the chronostratigraphy of the southern laterites, particularly the reticulated
48 laterites (Huang, 1993; Huang et al., 1996; Li and Gu, 1997; Wu et al., 2000; Yuan et al., 2008;
49 Zhang et al., 2008; Zhang et al., 2020; Zheng et al., 1979).

50 The composition and lithology of the parent material control the characteristics of the
51 weathering crusts leading to the formation of various kinds of weathering crusts. The sedimentary
52 facies of the reticulated laterites in South China can be divided into fluvial, littoral, and aeolian
53 (Yuan et al., 2008). Fluvial deposits (fluvial facies) are extensively distributed along the banks of
54 rivers in southern China, and some of them have developed a deep weathered red crust and a
55 distinct reticulated red soil layer; therefore, they are often called reticulated laterites. In the early
56 1970s, Zheng et al. (1979) determined the fission-track ages of glass meteorites buried in red sand
57 dunes, Hainan Island, which originated in the Middle Pleistocene. Red sandy deposits (littoral
58 facies) are extensively distributed across the platform in the southeastern coastal area, most of
59 which comprise beach and coastal aeolian sands. After weathering occurred, the upper parts of
60 these sediments developed red, brownish-red, or even netted laterite. Geologically, these sandy
61 deposits are generally called “old red sands”. Zeng et al. (1999) and Wu et al. (2000) conducted
62 in-depth research on the old red aeolian sands on the southeastern coast and determined their age
63 to be less than 60 ka by thermoluminescence. In recent years, new optically stimulated
64 luminescence (OSL) data have indicated that the age at the base of the old red sands has exceeded
65 100 ka (Jin et al., 2018b; Zheng et al., 2021). Since 2000, in addition to further studies on the
66 chronostratigraphy of laterites in southern China, many scholars have begun to explore and extract
67 the environmental information contained in these deposits (Jiang et al., 2010; Lai H., 2017; Zhang
68 et al., 2020). Whether we can obtain effective environmental change information from laterite
69 profiles in South China depends on the in-depth study of laterite formation mechanisms and the
70 development of dating technology in South China. Can typical reticulated laterite be used as a
71 marker for climate stratigraphy and chronostratigraphy, or is it only of petrostratigraphic
72 significance?

73 In short, laterite in South China has become a new focus of Cenozoic geological and
74 environmental research in China. In recent years, an increasing number of Paleolithic sites have
75 been discovered in the laterites in South China, and it is crucial to determine their ages. This paper
76 focuses on the reticulated fluvial laterites found in the humid subtropical mountainous areas of
77 South China and their Paleolithic sites and provides a robust chronological framework of these
78 reticulated laterites under the influence of paleohuman activities and their implications for the
79 development of reticulated laterites in South China.

80 2. Study area

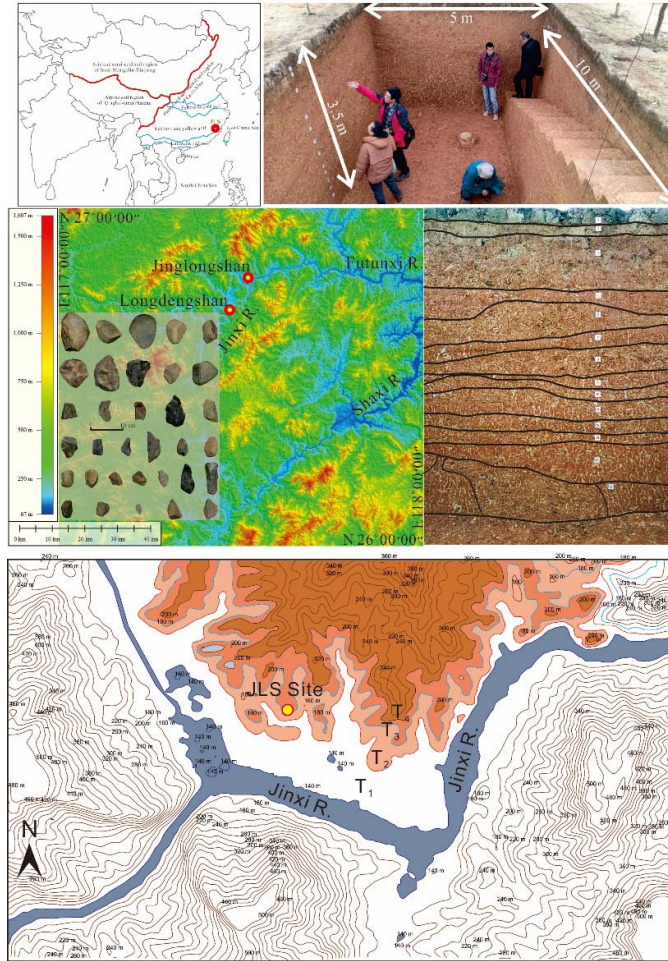
81 The Jinglongshan Paleolithic site (JLS) (26°46'41" N, 117°30'17" E), discovered in Jiangle
82 County, Fujian Province, is located at the southeastern foot of the Wuyi Mountains that are
83 oriented in a northeast-southwest direction, similar to the Jinxi River—the largest tributary of the

84 Futunxi River (Jin et al., 2021a). The JLS is located on the third fluvial terrace of the Jinxi River
85 (Fig. 1). This fluvial terrace is a pedestal terrace, and ~4-m-thick fluvial deposits have
86 accumulated on the severely weathered granite pedestal, including slope deposits originating from
87 the surrounding hills and mountains. After long-term weathering in a humid subtropical monsoon
88 climate, the sediments exhibit characteristics of red, brownish-red mixed with white, and
89 gray-white worm-like reticulate textures. Over the past 50 years, no more than 10 Paleolithic sites
90 have been discovered and formally excavated in Fujian Province (covering an area of more than
91 12×10^4 km²). Among these, only four sites have produced viable scientific dating data. The ages
92 of the rest of the sites can be estimated primarily through a comparison of stone tool-making
93 technology and the relative ages of adjacent geological strata. The JLS is a critical and
94 scientifically excavated open-air site dating from the Middle Paleolithic Period located in Fujian
95 Province. The discovery of the JLS expanded the distribution range of Paleolithic cultural relics in
96 Fujian Province and provided materials for comparing Paleolithic cultural properties in different
97 regions of South China. A chronological study of the strata not only provides an accurate
98 archaeological date for the site but also determines the minimum time required for the formation
99 of reticulated laterite under the humid East Asian monsoon climate.

100 **3. Materials and methods**

101 **3.1 Sampling**

102 The sampling section in Figure 1 can be divided into 15 layers from an archaeological
103 perspective (Fig. 1d). During the field surveys undertaken in September 2018, the JLS laterite
104 profile of ~50 m² (Fig. 1d) was investigated in detail. The 330-cm-thick laterite overlying alluvial
105 gravel can be subdivided into five lithological units (Fig. 1d). Unit 1 (330–260 cm) primarily
106 comprises dense, thick reticulated laterite; Unit 2 (260–150 cm) comprises sparse, thick reticulated
107 laterite; Unit 3 comprises three sublayers (the upper and lower layers are dense fine reticulated
108 laterite situated between a layer of sparse fine reticulated laterite); Unit 4 (80–30 cm) comprises a
109 weakly developed fine reticulated laterite layer. The plowing layer is situated at the top. Sixteen
110 OSL samples were collected from the east and west profiles of the pit by hammering a 20-cm-long
111 steel cylinder (with a diameter of 5 cm) into the freshly cleaned section (Fig. 2). The tubes were
112 then light-tightly wrapped in a black plastic bag.



113
 114 Figure 1. Location and profiles of the Jinglongshan Paleolithic site (JLS), South China. (a). Soil zone of the JLS
 115 and the zonal spatial distribution of soil in China; (b). A topographic map of the area where the JLS is located and
 116 typical stone tools are unearthed; (c–d). Macroscopic characteristics of the site pits and the characteristics of the
 117 reticulated laterite profile. (e). Topographic map of study area.

118 **3.2 Grain size analysis**

119 The grain size distributions of the OSL samples were determined to aid a better understanding
 120 of their sedimentary characteristics. The sediment was first treated with 30% H₂O₂ to remove any
 121 organic material and then with 10% HCl to remove any carbonates. The samples were then
 122 deflocculated using a 0.05 M (NaPO₃)₆ solution before being measured using a Malvern
 123 Mastersizer 2000 laser grain size analyzer.

124 **3.3 OSL dating**

125 Over the last 20 years, OSL dating has become one of the most extensively used numerical
 126 methods for determining burial ages in Late Quaternary sediments from a variety of depositional
 127 environments, such as loess (Constantin et al., 2021; Song et al., 2015), lacustrine deposits (Huang
 128 et al., 2021), aeolian dunes (Zheng et al., 2021), old red sands (Alappat et al., 2016; Jin et al.,
 129 2018b; Zhang et al., 2008), and sediments from prehistoric settlement sites (E et al., 2015; Jin et
 130 al., 2021b; Jin et al., 2018c; Zheng et al., 2018). The burial time of quartz and feldspar grains can

131 be estimated from the intensity of the OSL signal by converting it into an equivalent dose (D_e) and
132 dividing this D_e by the environmental dose rate.

133 Sample preparation and OSL measurements were performed at the Luminescence Dating
134 Laboratory of the FNU (Fuzhou, China). Under subdued red light in the laboratory, sediments at
135 each end of the sample tubes were scraped out for water content and dose rate measurements. The
136 sediments in the middle of the tubes were wet-sieved to extract the 63–90 μm fractions and were
137 then treated with 30% H_2O_2 and 10% HCl to remove organic and carbonate matter, respectively.
138 The 63–90 μm coarse grain fraction was then separated. Subsequently, the separated polymineral
139 fraction was etched with 30% H_2SiF_6 for one week to dissolve the feldspars, followed by
140 treatment with 10% HCl to remove any fluorides. The purity of the isolated quartz was checked
141 using the infrared (IR) depletion ratio method (Duller, 2003; Long et al., 2015); no significant IR
142 signals were observed in any of the samples. OSL measurements were performed using an
143 automated luminescence reader (Risø TL/OSL DA-20) equipped with blue light stimulation units
144 (470 ± 20 nm) and IR light (870 ± 40 nm). Irradiation was carried out using a ^{90}Sr beta source
145 (dose rate of 0.09 Gy/s) built into the reader (Jin et al., 2021b). The quartz OSL signal was
146 detected using a photomultiplier tube through a 7.5-mm-thick U-340 filter.

147 To select appropriate measurement conditions for the D_e determination, preheat plateau and
148 dose recovery tests were conducted using the representative sample FNU2019056. The preheat
149 temperature varied from 180 $^\circ\text{C}$ to 280 $^\circ\text{C}$ (for 10 s) with an interval of 20 $^\circ\text{C}$, and the cut heat
150 was kept constant at 160 $^\circ\text{C}$ (Fig. 2b). Three aliquots were measured for each temperature. A dose
151 recovery test for various preheat temperatures was performed on the same representative sample
152 (Fig. 2c).

153 For dose rate determination, the U and Th concentrations were measured using inductively
154 coupled plasma mass spectrometry (ICP-MS), and the K concentration was measured using
155 atomic absorption spectrometry (AAS). The radionuclide concentrations were converted using the
156 conversion factors of (Guérin et al., 2011). The cosmic contribution was calculated according to
157 (Prescott and Hutton, 1994), based on the geomagnetic latitude and burial depth of the samples.
158 The moisture content was estimated to be $10 \pm 5\%$ for all samples, allowing for temporal
159 fluctuations during the burial of the sediments from the humid subtropical area.

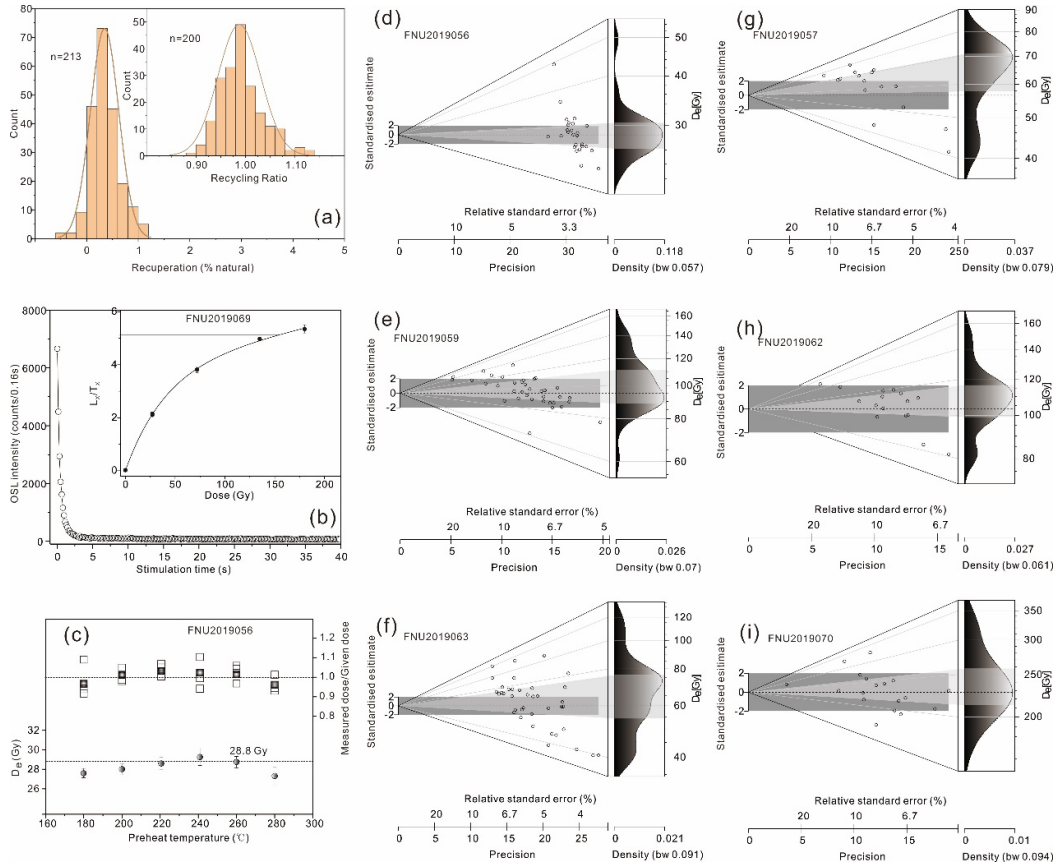
160 4. Results

161 4.1 Luminescence characteristics

162 Figure 2b depicts the decay curve for the representative sample (FNU2019069). The OSL
163 signals rapidly decreased and approached the background level during the first few seconds of
164 stimulation. The fast component accounted for $\sim 80\%$ of the initial natural signal and dominated
165 the first 0.80 s signal that was integrated for D_e determination. The growth curve can be well fitted
166 by a single saturating exponential function (Fig. 2b).

167 The results of the preheat plateau and dose recovery tests for sample FNU2019056 are shown in
168 Figure 2c. A D_e plateau was observed for the preheat temperatures ranging from 220 $^\circ\text{C}$ to 280 $^\circ\text{C}$,
169 while the recycling ratios were within 10% of unity for all preheat temperatures. The dose
170 recovery and recycling ratios of the dose recovery test generally ranged between 0.9 and 1.1,
171 exhibiting a trend similar to that of the preheat plateau test. Hence, we chose a preheat temperature

172 of 260 °C with a cut-heat of 160 °C for all D_e determinations. The dose recycling ratios and
 173 recuperations of all the samples tested under the chosen measurement conditions are shown in
 174 [Figure 2a](#). Most of the dose recycling ratios ranged from 0.9 to 1.1 with a mean of 0.967 ± 0.005 ,
 175 and most of the recuperations were less than 1% of the natural signal.



176
 177 [Figure 2](#). (a). Recycling ratio and recuperation data for all samples; (b). OSL stimulation curve for aliquots of
 178 sample 2019069 for which the inset curve is fitted with a single saturating exponential function ($I = I_0(1 -$
 179 $\exp[-(D)/D_0])$); (c). Preheat plateau and dose recovery test results for sample 2019056; (d–i). Abanico plots and
 180 frequency density diagrams depicting the distribution of the D_e s values of six typical OSL samples.

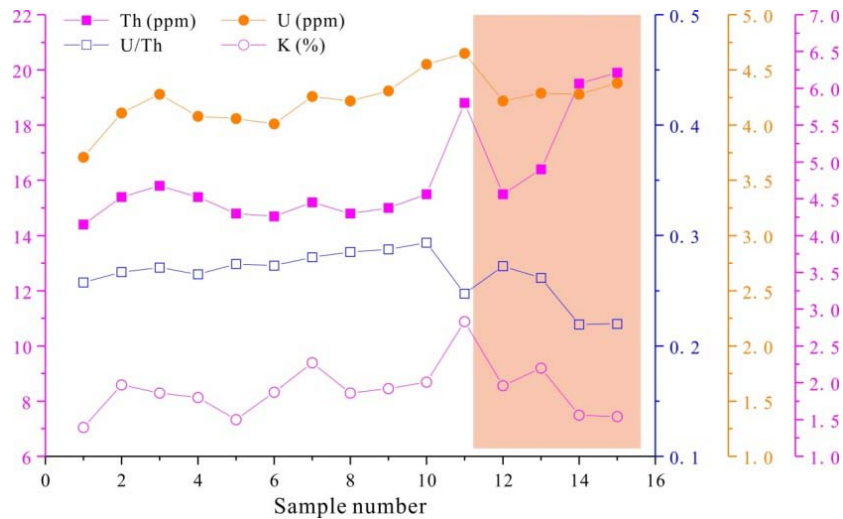
181 4.2 Environmental dose rate and age estimation

182 The environmental dose rate, as one of two main parameters, can have a significant impact on
 183 the calculation of OSL ages ([Adamiec and Aitken, 1998](#); [Zhao and Li, 2002](#)). The dose rates of the
 184 16 OSL samples ranged between 3.21 ± 0.16 Gy/ka and 5.02 ± 0.27 Gy/ka ([Table 1](#)). The U/Th
 185 rate and K, U, and Th contents for all the OSL samples from the JLS are shown in [Figure 3](#). The
 186 lower part of the JLS profile comprises typical dense, thick, reticulated laterite sediments situated
 187 in the humid subtropical areas of South China. For the samples (FNU2019067–2019070) from the
 188 lower part of the JLS profile, the U content (4.22 ± 0.09 $\mu\text{g/g}$ and 4.38 ± 0.09 $\mu\text{g/g}$) did not change
 189 significantly, but the Th content (15.5 ± 0.28 $\mu\text{g/g}$ and 19.9 ± 0.26 $\mu\text{g/g}$) and dose rate (3.80 ± 0.20
 190 Gy/ka and 5.02 ± 0.22 Gy/ka) were much higher than those of the samples from the upper part of
 191 the profile.

192 To understand the chemical weathering characteristics of the JLS profile, we compared the old
 193 reticulated red sands from the coastal area of South China ([Jin et al., 2018a](#); [Zhang et al., 2008](#))

194 with the reticulated laterites from the Paleolithic sites in central China (Zhang et al., 2019) and
 195 South China (Jin et al., 2021a), and found differences in the U/Th ratio and K content. During soil
 196 formation, U and Th are redistributed due to weathering, and the leaching rates of U and Th are
 197 different; therefore, their ratio can effectively indicate chemical weathering intensity (Gueniot et
 198 al., 1988a; Gueniot et al., 1988b). Compared with the Paleolithic reticular laterite in subtropical
 199 Hunan Province (Zhang et al., 2019), the overall weathering intensity of the JLS profile was lower
 200 than that of the reticular laterite in central China and much lower than that of the Late Pleistocene
 201 red sands in coastal Fujian Province (Jin et al., 2018b), but close to that of the reticular laterite at
 202 the Longdengshan Paleolithic site (Jin et al., 2021a). The abovementioned weathering
 203 characteristics may indicate that the U and Th contents of the JLS profile are relatively stable, and
 204 the element activation and migration caused by weathering have little influence on the reliability
 205 of the OSL age; in other words, the burial age estimated by the single-aliquot regenerative-dose
 206 (SAR) method can effectively indicate the formation time of regional reticular laterites.
 207 Specifically, the chemical weathering intensity indicated by the U/Th ratio of the sediments in the
 208 upper part (0.40–2.25 m) of the section gradually decreased from top to bottom, and the trend
 209 changed at 2.25 m. Chemical weathering of the 2.25–3.3 m section was stronger than that of the
 210 0.4–2.25 m section overall and exhibited an increasing trend with depth, which was not simply a
 211 variation characteristic purely attributable to weathering intensity in the natural environment, and
 212 was highly likely to be influenced by other factors. The most likely factor is human activity. The
 213 long-term influence of human activities causes the active surface to undergo long-term weathering
 214 and changes according to the intensity of the aforementioned human activities. The
 215 above-mentioned characteristics correspond to the cultural layer of the site, which also represents
 216 the primary period of ancient human activity at the site.

217



218

219

Figure 3. U/Th rate and the K, U, and Th contents for all the OSL samples from the JLS.

220

221

Table 1. Summary of the U, Th, and K contents and the dose rates values for the reticulated laterite sediments.

Lab. number	Depth (m)	Sediment sequence	Aliquots	Grain size (μm)	Th (μg/g)	U (μg/g)	K (%)	Water content (%)	Cosmic rate (Gy/ka)	Dose Rate (Gy/ka)
FNU19056	0.40	3	26	63-90	14.4	3.71	1.39	10±5	0.23 ± 0.02	3.21 ± 0.16
FNU19057	0.65	4	13	63-90	15.4	4.11	1.97	10±5	0.22 ± 0.02	3.91 ± 0.02

FNU19058	1.00	5	13	63-90	15.8	4.28	1.86	10±5	0.22 ± 0.02	3.89 ± 0.20
FNU19059	1.30	6	16	63-90	15.4	4.08	1.8	10±5	0.21 ± 0.02	3.76 ± 0.20
FNU19060	1.50	7	16	63-90	14.8	4.06	1.5	10±5	0.21 ± 0.02	3.43 ± 0.17
FNU19061	1.65	9	17	63-90	14.7	4.01	1.87	10±5	0.2 ± 0.02	3.75 ± 0.20
FNU19062	1.75	10	38	63-90	15.2	4.26	2.27	10±5	0.17 ± 0.02	4.19 ± 0.22
FNU19063	1.75	10	36	63-90	14.8	4.22	1.86	10±5	0.18 ± 0.02	3.78 ± 0.19
FNU19064	1.90	11	17	63-90	15	4.31	1.92	10±5	0.18 ± 0.02	3.86 ± 0.2
FNU19065	2.10	12	16	63-90	15.5	4.55	2.01	10±5	0.16 ± 0.01	3.95 ± 0.22
FNU19066	2.25	13	16	63-90	18.8	4.65	2.83	10±5	0.18 ± 0.02	5.02 ± 0.27
FNU19067	2.40	14	14	63-90	15.5	4.22	1.96	10±5	0.18 ± 0.02	4.19 ± 0.22
FNU19068	2.70	15	18	63-90	16.4	4.29	2.2	10±5	0.17 ± 0.02	4.19 ± 0.22
FNU19069	2.80	15	17	63-90	19.5	4.28	1.56	10±5	0.17 ± 0.02	3.80 ± 0.20
FNU19070	3.30	15	18	63-90	19.9	4.38	1.54	10±5	0.17 ± 0.02	3.84 ± 0.20

222

223 The quartz OSL dating results are summarized in Table 2, and the D_e s ranged between 28.76 ±
 224 0.82 Gy and 232.64 ± 8.78 Gy. The D_e s of quartz was determined using a combination of SAR
 225 protocols (Murray and Wintle, 2000). The over-dispersion of D_e s for each sample was calculated
 226 using the central age model (CAM) (Galbraith et al., 1999), while the maximum age model was
 227 used to calculate MaxAM D_e s (Galbraith and Roberts, 2012). A sigma-b value of 0.15 was used
 228 for the single aliquot samples. Bayesian age-depth modeling was performed using the Bacon code
 229 (Blaauw and Christen, 2011) in the R package, based on the 16 OSL ages of the JLS profile.

230 Table 2. Summary of the equivalent dose values (D_e) and optically stimulated luminescence (OSL) ages (Age) for
 231 the reticulated laterite sediments.

Lab. number	Depth (m)	Sediment sequence	D_e (Gy)	Max D_e (Gy)	OD (%)	CAM Age (ka)	MaxAM Age (ka)
FNU19056	0.40	3	28.76 ± 0.82	29.98 ± 2.40	14 ± 2	8.97 ± 0.52	9.29 ± 0.89
FNU19057	0.65	4	69.08 ± 2.81	72.40 ± 4.03	13 ± 3	17.65 ± 0.76	18.53 ± 1.41
FNU19058	1.00	5	94.48 ± 8.59	103.06 ± 7.45	32 ± 7	24.28 ± 2.55	26.80 ± 2.43
FNU19059	1.30	6	105.76 ± 3.76	108.31 ± 6.38	11 ± 3	28.13 ± 1.79	28.91 ± 2.28
FNU19060	1.50	7	108.18 ± 10.19	109.25 ± 4.30	6 ± 3	31.51 ± 3.35	31.81 ± 2.05
FNU19061	1.65	9	131.69 ± 17.31	134.80 ± 6.46	7 ± 4	35.14 ± 5.00	36.04 ± 2.43
FNU19062	1.75	10	64.29 ± 3.01	83.57 ± 6.49	28 ± 3	15.33 ± 1.10	21.89 ± 2.03
FNU19063	1.75	10	98.41 ± 2.65	100.54 ± 4.09	14 ± 2	26.06 ± 1.46	26.80 ± 1.84
FNU19064	1.90	11	39.58 ± 4.92	66.47 ± 8.19	51 ± 9	10.25 ± 1.36	17.31 ± 2.27
FNU19065	2.10	12	82.09 ± 5.13	89.08 ± 6.25	24 ± 5	20.80 ± 1.71	22.23 ± 1.92
FNU19066	2.25	13	61.35 ± 3.13	69.02 ± 4.49	19 ± 4	12.23 ± 0.9	13.83 ± 1.15
FNU19067	2.40	14	82.54 ± 7.66	115.22 ± 15.23	28 ± 8	19.69 ± 2.2	29.69 ± 4.31
FNU19068	2.70	15	94.22 ± 6.5	171.66 ± 33.11	28 ± 5	22.48 ± 2.04	44.85 ± 8.98
FNU19069	2.80	15	150.72 ± 11.09	179.18 ± 18.93	29 ± 6	39.64 ± 3.62	47.41 ± 5.79
FNU19070	3.30	15	232.64 ± 8.78	237.49 ± 14.08	13 ± 3	60.65 ± 3.79	62.32 ± 4.89

232

233 **5. Discussion**

234 **5.1 Impact of weathering on environmental dose rate**

235 Reticulation in laterite is the result of differential weathering. The reticulate character is formed
236 based on a red soil substrate and is closely related to abundant rainfall. The reported results
237 indicate that the reticulated laterite in South China is the product of chemical weathering under the
238 humid and hot climate conditions of the Late Pleistocene, and its development age is more than
239 300 ka. However, the ages of the reticulated laterites developed from different parent materials
240 were different. For example, the reticulated laterites of Lushan Mountain in Jiujiang, Jiangxi
241 Province, and the Baise Basin in Guangxi are formed by the weathering of rocks, and the reported
242 fission-track ages range from 0.3 to 0.7 Ma. The old reticulated red sands (littoral facies) are
243 generally believed to have been formed by re-transport of beach sand during the high sea level
244 period related to deep-sea oxygen isotope stage 5, with a typical age of less than 0.2 Ma. In China,
245 the formation age of reticulated laterite as a fluvial facies has not been reported.

246 Mineralogical analysis of the lateritic clay in South China shows that there is no bauxite in the
247 clay assemblage, and even the small amount of 2:1 clay minerals present, such as vermiculite,
248 indicates that the lateritic clay did not experience the lateritic process in humid tropical regions.
249 This indicates that the formation of reticulated laterites in both the subtropics and the subtropics is
250 in the moderate to strong chemical weathering stage, and the formation of reticulated laterites does
251 not require extremely strong chemical weathering. Combined with the dating results, it can be
252 seen that, in the fluvial laterites of South China, dense thick dendritic reticulation can be formed
253 by at least 60 ka, and the time required for the beginning of reticulation is even shorter, requiring
254 less than 10 ka. Therefore, reticulated laterites cannot be used as markers of climate and
255 chronostratigraphy. Under normal circumstances, the contents of U and Th deposited naturally are
256 affected by leaching under hydrothermal conditions, and their contents gradually decrease from
257 top to bottom. However, the contents of U and Th in the JLS profile gradually increased from top
258 to bottom, and there was a distinct turning point near the depth of 2.25 m, which divides the
259 profile into two main stages. The 2.25-m-deep layer may indicate a stable surface of human
260 activity of a long duration, and the effect of time on weathering is less than that of human activity
261 intensity; therefore, the 2.25–3.3-m-deep layer represents an abnormal chemical weathering trend.
262 The multiple layers between the 2.25-m- and 0.4-m-deep layers indicate that each period of human
263 activity was relatively short, and the effect of human activity intensity on weathering was less than
264 that of time, indicating a normal chemical weathering trend. As discussed in the previous section,
265 the formation time of fluvial reticulated laterite in South China does not require tens of thousands
266 or hundreds of thousands of years but it can be formed within tens of thousands or even ten
267 thousand years under appropriate hydrothermal conditions.

268 In contrast to the weathering process of natural sediments, each cultural sediment layer at the
269 Paleolithic site is a surface representing human activity during a specific period, and its chemical
270 weathering intensity process is a function of the hydrothermal conditions, human activity intensity,
271 time, and natural deposition rate. Generally, a dense coarse texture indicates a high degree of
272 chemical weathering, whereas sparse coarse and fine textures indicate relatively low chemical
273 weathering intensity. However, for loose deposits disturbed by human activities, the thickness, and
274 density of the reticulation are ineffective indicators of the chemical weathering rate. The intensity

275 and duration of human activity can affect the degree of chemical weathering of reticulated laterites.
276 The shorter the duration and intensity of human activities, the lower their contribution to chemical
277 weathering. In contrast, the longer and more intense human activities are, the greater their
278 influence on chemical weathering. Therefore, what is the coupling relationship between chemical
279 weathering intensity and time? This scientific problem requires a more systematic analysis of
280 geochemistry and isochron luminescence chronology.

281

282 **5.2 OSL burial ages of the T3 reticular laterite terraces**

283 Bayesian methods have long been recognized as powerful aids in the analysis of age
284 information (Ramsey, 2009). Given the ability of Bayesian analysis to identify outliers and
285 increase precision, a total of 16 luminescence ages were eventually used to construct the Bacon
286 age-depth model with a 1 cm resolution using the R package Bacon (Blaauw and Christen, 2011).
287 The model was run using default or suggested settings, and the depth scale was divided into equal
288 30-cm-thick sections (thick = 30). The model was run to produce ages with a resolution of 10 cm.
289 Uncertainties in the age input data contained only random components. The Bayesian age model
290 exhibits an uncertainty of 1 sigma (gray shadow) in Figure 4, together with the interpolated model
291 ages (with total uncertainties) at the formation boundaries. Although there are several reversed
292 ages, the OSL ages are generally inconsistent with the stratigraphic order and vary between 60.65
293 ± 3.76 ka and 8.97 ± 0.52 ka, with an apparent age gap and substantially decreased between ~ 6 ka
294 and ~ 2 ka.

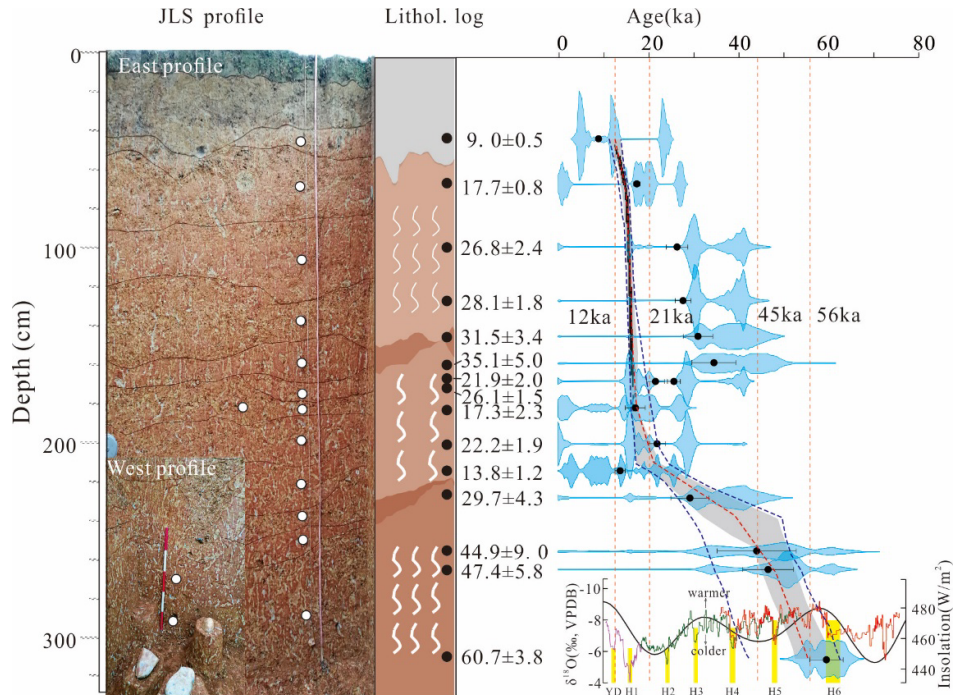
295 The dating results of the reticulated red soil layer of the T3 terrace indicate that paleohuman
296 activity entered its most prosperous period ~ 60 – 40 ka ago, which indicates that ancient activities
297 in the Jiangle Basin were significantly delayed. Compared with previous studies (Fan et al., 2019;
298 Wang, 1997), this is the first systematic dating of the independent age of Paleolithic sites in the
299 hilly and mountainous areas of western Fujian Province and provides a critical chronology for
300 understanding the evolution of Paleolithic technology and human behavior in this area. This result
301 is consistent with the age of the adjacent Longdengshan Paleolithic site that has been formed
302 during the Late Pleistocene and exhibits definite buried strata (Jin et al., 2021a). In previous
303 studies (Fan et al., 2019; Wang, 1997), the ages of the Paleolithic sites in South China were
304 inferred from stone tool-making technology and the reticulate laterites developed by buried strata
305 are still questionable, and they are most likely not the sites that originated during the Middle
306 Pleistocene and early Late Pleistocene, but the sites that originated during the middle and late
307 Pleistocene.

308 Studies have shown that laterites in China have experienced multiple developmental stages.
309 Under the influence of a strong summer monsoon, a red weathering crust is extensively developed
310 in South China. Under the combined influence of the summer monsoon climate and tectonic uplift,
311 the fluvial geomorphology of the Jinxi River is characterized by erosion on one side and
312 accumulation on the floodplain on the other side, until the floodplain reaches the upper limit of the
313 alluvial deposits. The sedimentary processes of the JLS section can be divided into three sections
314 according to the age-depth model; 56 – 45 ka (rapid accumulation stage, 4.5 cm/ka), 45 – 21 ka
315 (slow accumulation stage, 2.6 cm/ka), and 21 – 11 ka (rapid accumulation stage, 16.7 cm/ka)
316 sections, as shown in Figure 4.

317 Based on chronological data, the lateral accretion rates of the lateral erosion and raised bank

318 were calculated. The results indicated that the average cutting and lateral accretion rates of the
319 first and second terraces were 1.2–3 m/ka and 30–110 m/ka, respectively. The average cutting rate
320 and lateral erosion rate of the three echelon terraces were 0.43 m/ka and 4.26 m/ka, respectively,
321 and the cutting rate varied between stages.

322 As can be seen from the diachronism of strata (Fig. 5), the sedimentation rate is closely related
323 to the flood frequency of the river terraces, and the flood processes in South China primarily
324 originate from summer precipitation. Existing studies indicate that the regional summer
325 precipitation is primarily affected by the East Asian summer monsoon; therefore, the
326 sedimentation rate in the JLS profile should theoretically be closely related to variations in the
327 East Asian summer monsoon. By comparing the $\delta_{18}\text{O}$ isotopic records of the stalagmites in Hulu
328 Cave (Wang et al., 2008), it was found that the three sedimentary stages have a significant
329 relationship with global and regional hydrothermal changes, and the two nodes with the most
330 significant variations in deposition rate are located in the valley that receives the highest solar
331 radiation intensity. Several abrupt climatic events since MIS3 have promoted the regional soil
332 erosion rate (Fig. 4). Changes in hydrothermal conditions can lead to changes in vegetation, soil
333 erosion, river water volume, and sediment sources, all of which affect river accretion and
334 downcutting. Fluvial downcutting primarily occurred during the stable and humid climate period,
335 whereas accretion occurred during the distinct climate transition period. The comparison results
336 showed that the greater the variability of summer monsoon intensity, the greater the deposition
337 rate; that is, the greater the variability of summer monsoon intensity, the more it affected the
338 erosion–transport–deposition rate in the region. This has been confirmed by other studies (Li et al.,
339 2018). Under stable and warm climates, precipitation is abundant, leading to substantial river
340 water volumes. However, owing to the weaker cold and frost weathering and the increase in
341 surface vegetation, the sediment source in the river has been reduced and the transport effect is
342 strong, which primarily manifests as shear erosion. When the climate fluctuates from cold to warm,
343 the situation is different; river flood action is stronger, and the sediment source is rich and easily
344 accumulates. A similar phenomenon occurs when the climate transitions from warm to cold.
345 Therefore, the strong period of river accumulation is mostly the result of alternating periods of
346 cold and hot climates.

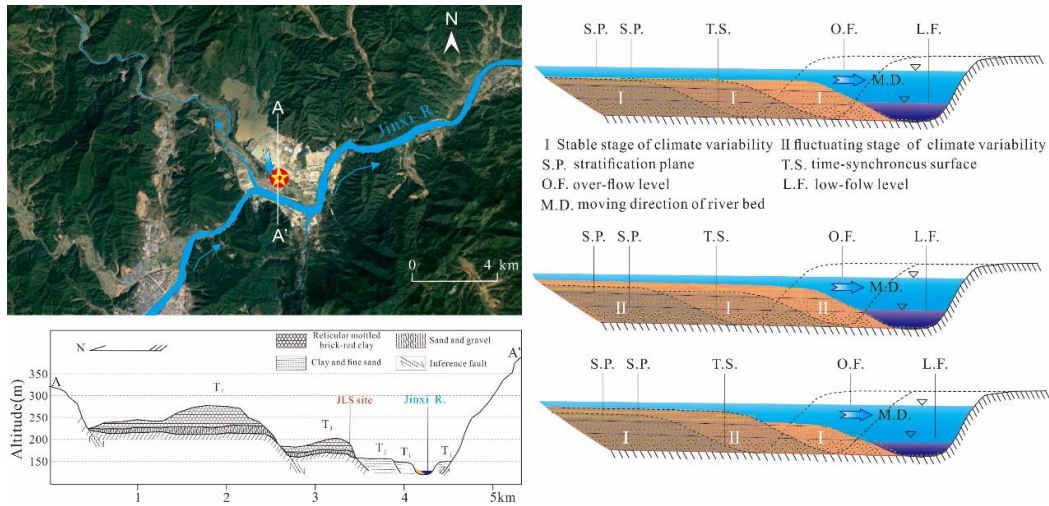


347
348
349
350

Figure 4. (a). Stratigraphy and chronology of the investigated profile; (b). OSL age-depth relationships for the JLS profile. Median ages (red line) and the 95% probability age range (gray shadow) for the section are based on a Bacon age-depth model.

351
352
353

The measured age data were inconsistent with the stratigraphic sequence rate (Fig. 4). This may be related to the diachronism of the river bank strata (Fig. 5), in addition to the error in the test and overestimation of the age caused by uneven sunning of the samples.



354
355
356

Figure 5. Sketch of the stratigraphic diachronism of terrace deposition.

357

6. Conclusion

358
359

The T3 terrace, an archive of hominin activity in the study area, primarily formed between 56 and 11 ka. Terraces T1 and T2 of the Jinxi River have formed since the Holocene, which is

360 consistent with the existing period of regional hominin activity.

361 Reticulated laterite cannot be used simply to determine the ages of the Paleolithic sites found in
362 this stratum. It should be analyzed and judged according to the provenance type and
363 geomorphology of the reticulated laterite. Typical reticulated laterite cannot be used as a marker
364 for climatic stratigraphy and chronostratigraphy. The formation time of the reticulated laterite
365 varied significantly between different sedimentary facies. Among them, the formation time of the
366 fluvial reticulated laterite in the southern tropics did not require tens of thousands of years or even
367 hundreds of thousands of years. Therefore, under suitable hydrothermal conditions, reticulated
368 laterite can form within tens of thousands of years or even within 10 ka.

369 Human activities, indicated by settlement sites, can affect the burial age of reticulated red soil,
370 and the temporal nature of riverine terraces can also lead to an inversion in the age of reticulated
371 red soil.

372

373 Adamiec, G. and Aitken, M., 1998. Dose-rate conversion factors update. *Ancient TL*, 16(2): 37-50.

374 Alappat, L., Joseph, S., Tsukamoto, S., Kaufhold, S. and Frechen, M., 2016. Chronology and weathering
375 history of red dunes (Teri Sands) in the southwest coast of Tamil Nadu, India. *Zeitschrift der*
376 *Deutschen Gesellschaft für Geowissenschaften*.

377 Blaauw, M. and Christen, J.A., 2011. Flexible paleoclimate age-depth models using an autoregressive
378 gamma process. *Bayesian Analysis*, 6(3).

379 Constantin, D., Mason, J.A., Veres, D., Hambach, U., Panaiotu, C., Zeeden, C., Zhou, L., Marković, S.B.,
380 Gerasimenko, N., Avram, A., Tecsa, V., Groza-Sacaciu, S.M., del Valle Villalonga, L., Begy, R.
381 and Timar-Gabor, A., 2021. OSL-dating of the Pleistocene-Holocene climatic transition in
382 loess from China, Europe, and North America, and evidence for accretionary pedogenesis.
383 *Earth-Science Reviews*, 221.

384 Duller, G.A.T., 2003. Distinguishing quartz and feldspar in single grain luminescence measurements.
385 *Radiation Measurements*, 37(2): 161-165.

386 E, C., Lai, Z., Hou, G., Cao, G., Sun, Y., Wang, Y. and Jiang, Y., 2015. Age determination for a Neolithic
387 site in northeastern Qinghai-Tibetan Plateau using a combined luminescence and
388 radiocarbon dating. *Quaternary Geochronology*, 30: 411-415.

389 Fan, X., Zhou, Z., Wang, X., Huang, Y., Gao, H. and Chen, C., 2019. Brief report on the excavation of
390 Longdengshan Paleolithic site in west of Fujian Province, China(福建将乐龙灯山遗址试掘简
391 报). *Fujian wenbo(福建文博)*(3): 2-7.

392 Galbraith, R.F. and Roberts, R.G., 2012. Statistical aspects of equivalent dose and error calculation and
393 display in OSL dating: An overview and some recommendations. *Quaternary Geochronology*,
394 11: 1-27.

395 Galbraith, R.F., Roberts, R.G., Laslett, G.M., Yoshida, H. and Olley, J.M., 1999. Optical dating of single
396 and multiple grains of quartz from Jinmium Rock shelter, northern Australia: part 1,
397 experimental design and statistical models. *Archaeometry*, 41(2): 339-364.

398 Gueniot, B., Munier-Lamy, C. and Berthelin, J., 1988a. Geochemical behavior of uranium in soils, part I.
399 Influence of pedogenetic processes on the distribution of uranium in aerated soils. *Journal of*
400 *Geochemical Exploration*, 31(1): 21-37.

401 Gueniot, B., Munier-Lamy, C. and Berthelin, J., 1988b. Geochemical behavior of uranium in soils, part II.
402 Distribution of uranium in hydromorphic soils and soil sequences. Applications for surficial
403 prospecting. *Journal of Geochemical Exploration*, 31(1): 39-55.

-
- 404 Guérin, G., Mercier, N. and Adamiec, G., 2011. Dose-rate conversion factors: Update. *Ancient TL*, 29(1):
405 5-8.
- 406 Huang, C., Lai, Z., Liu, X. and Madsen, D., 2021. Lake-level history of Qinghai Lake on the NE Tibetan
407 Plateau and its implications for Asian monsoon pattern - A review. *Quaternary Science*
408 *Reviews*, 273.
- 409 Huang, Z., 1993. Comparison of the Paleodune formed during the Late Pleistocene between China and
410 Japan. *Tropical Geography*, 13(1): 1-12.
- 411 Huang, Z., Zhang, W. and Chen, J., 1996. *Weathering Crusts in South China*. Beijing: China Ocean Press,
412 1996. 1~312.
- 413 Jiang, J., Xu, R.-k. and Zhao, A.-z., 2010. Comparison of the surface chemical properties of four soils
414 derived from Quaternary red earth as related to soil evolution. *Catena*, 80(3): 154-161.
- 415 Jin, J.-h., Li, Z.-z., Cheng, Y., Xu, X.-l., Li, Z.-x. and Liu, X.-j., 2018a. Late Pleistocene aeolian activity in
416 Haitan Island, Southeast China: Insights from optically stimulated luminescence dating of
417 coastal dunes on marine terraces. *Journal of Mountain Science*, 15(8): 1777-1788.
- 418 Jin, J.-h., Wang, X.-y., Zhou, Z.-y., Huang, Y.-m., Fan, X.-c., Zuo, X.-x., Li, Z.-z., Ling, Z.-y., Ren, Y.-q. and Li,
419 S.-t., 2021a. OSL chronology of a Palaeolithic site in a humid subtropical mountainous area of
420 southeast China. *Journal of Mountain Science*, 18(8): 2012-2023.
- 421 Jin, J., Cai, X., Huang, Y., Zuo, X., Ling, Z., Dai, J., Ren, Y., Zhang, W. and Li, S., 2021b. New luminescence
422 dating evidence reveals the timing of Neolithic human activities in Fuzhou Basin, South China.
423 *Catena*, 207.
- 424 Jin, J., Li, Z., Cheng, Y., Xu, X., Li, Z. and Liu, X., 2018b. Late Pleistocene aeolian activity in Haitan Island,
425 Southeast China: Insights from optically stimulated luminescence dating of coastal dunes on
426 marine terraces. *Journal of Mountain Science*, 15(8): 1777-1788.
- 427 Jin, J., Li, Z., Huang, Y., Fan, X., Jiang, F., Cheng, Y., Xu, X., Ling, Z. and Liu, X., 2018c. Chronology of a
428 late Neolithic site along the coast of the east China sea. *Quaternary Geochronology*, 48:
429 171-179.
- 430 Lai H., L.Z., Jin J., Deng T., Jiang F., Yuan X., Shen J., Yu X., Xu X., Cheng Y., 2017. Sedimentary structure
431 and developing model of coastal alluvial fan along the northern coast of Haitan Island, Fujian.
432 *Acta Geologica Sinica*, 91(8): 1878-1893.
- 433 Li, C.a. and Gu, Y., 1997. Stratigraphic study on the vermicular red earth at Xiushui County, Jiangxi
434 Province. *Journal of Stratigraphy*, 21(3): 226-232.
- 435 Li, G., Chen, F., Xia, D., Yang, H., Zhang, X., Madsen, D., Oldknow, C., Wei, H., Rao, Z. and Qiang, M.,
436 2018. A Tianshan Mountains loess-paleosol sequence indicates anti-phase climatic variations
437 in arid central Asia and in East Asia. *Earth and Planetary Science Letters*, 494: 153-163.
- 438 Long, H., Haberzettl, T., Tsukamoto, S., Shen, J., Kasper, T., Daut, G., Zhu, L., Mäusbacher, R. and
439 Frechen, M., 2015. Luminescence dating of lacustrine sediments from Tangra Yumco
440 (southern Tibetan Plateau) using post-IR IRSL signals from polymineral grains. *Boreas*, 44(1):
441 139-152.
- 442 Murray, A.S. and Wintle, A.G., 2000. Luminescence dating of quartz using an improved single-aliquot
443 regenerative-dose protocol. *Radiation Measurements*, 32(1): 57-73.
- 444 Prescott, J.R. and Hutton, J.T., 1994. Cosmic ray contributions to dose rates for luminescence and ESR
445 dating: Large depths and long-term time variations. *Radiation Measurements*, 23(2-3):
446 497-500.
- 447 Ramsey, C.B., 2009. Bayesian Analysis of Radiocarbon Dates. *Radiocarbon*, 51(1): 337-360.

448 Song, Y., Lai, Z., Li, Y., Chen, T. and Wang, Y., 2015. Comparison between luminescence and
449 radiocarbon dating of late Quaternary loess from the Ili Basin in Central Asia. *Quaternary*
450 *Geochronology*.

451 Wang, Y., 1997. 更新世环境与中国南方旧石器文化发展. Peking University Press, Beijing.

452 Wang, Y., Cheng, H., Edwards, R.L., Kong, X., Shao, X., Chen, S., Wu, J., Jiang, X., Wang, X. and An, Z.,
453 2008. Millennial- and orbital-scale changes in the East Asian monsoon over the past 224,000
454 years. *Nature*, 451(7182): 1090-3.

455 Wu, Z., Wang, W., Tan, H. and Xu, F., 2000. The chronology of old red sand along the coast of west
456 Guangdong and south Fujian, China. *Science Bulletin*, 45(5): 533-537.

457 Yuan, B., Xia, Z., Li, B., Qiao, Y., Gu, Z., Zhang, J., Xu, B., Huang, W. and Zeng, R., 2008.
458 Chronostratigraphy and stratigraphic division of red soil in Southern China. *Quaternary*
459 *Sciences*, 28(1): 1-13.

460 Zeng, C., Chen, J. and Wu, Y., 1999. Research on the old red sands along the coast of southeast Fujian.
461 Geological Publishing House, Beijing.

462 Zhang, J.-F., Li, Y.-Y., Han, Y.-S. and Wang, J.-K., 2019. Luminescence dating of weathered sediments
463 from the Paleolithic site of Fengshuzui in northern Hunan province, China. *Quaternary*
464 *Geochronology*, 49: 211-217.

465 Zhang, J., Yuan, B. and Zhou, L., 2008. Luminescence chronology of "Old Red Sand" in Jinjiang and its
466 implications for optical dating of sediments in South China. *Chinese Science Bulletin*, 53(4):
467 591-601.

468 Zhang, X., Zhu, L., Huang, Y., Li, F., Xiong, W., Jia, J., Wang, T. and Ye, W., 2020. The reticulated
469 mechanism and its climatic implication of aggradation red earth. *Quaternary Sciences*, 40(1):
470 214-228.

471 Zhao, H., and Li, S.H., 2002. Luminescence Isochron Dating: A New Approach with Different Grain Sizes.
472 *Radiation Protection Dosimetry*, 101(1): 333-338.

473 Zheng, F., Li, Z., Jin, J., Zhang, W., Li, Z., Xu, X. and Cheng, Y., 2021. Luminescence geochronology and
474 paleoenvironmental implications of coastal red dune sands of northeast Hainan Island, China.
475 *Aeolian Research*, 53.

476 Zheng, H., Zhou, Y., Yang, Q., Hu, Z., Ling, G., Zhang, J., Gu, C., Wang, Y., Cao, Y., Huang, X., Cheng, Y.,
477 Zhang, X. and Wu, W., 2018. Spatial and temporal distribution of Neolithic sites in coastal
478 China: Sea level changes, geomorphic evolution, and human adaption. *Science China Earth*
479 *Sciences*, 60: 123-133.

480 Zheng, Y., Yuan, B. and Lianfang, Y., 1979. Fission track dating of Hainan tektite (Leigongmo). *Chinese*
481 *Journal of Geology*(1): 37-42.

482